




First-principles analysis of the detection of amine vapors using an antimonene electroresistive molecular device

R. Bhuvaneswari¹ · V. Nagarajan¹ · R. Chandiramouli¹ 

Published online: 18 May 2019

© Springer Science+Business Media, LLC, part of Springer Nature 2019

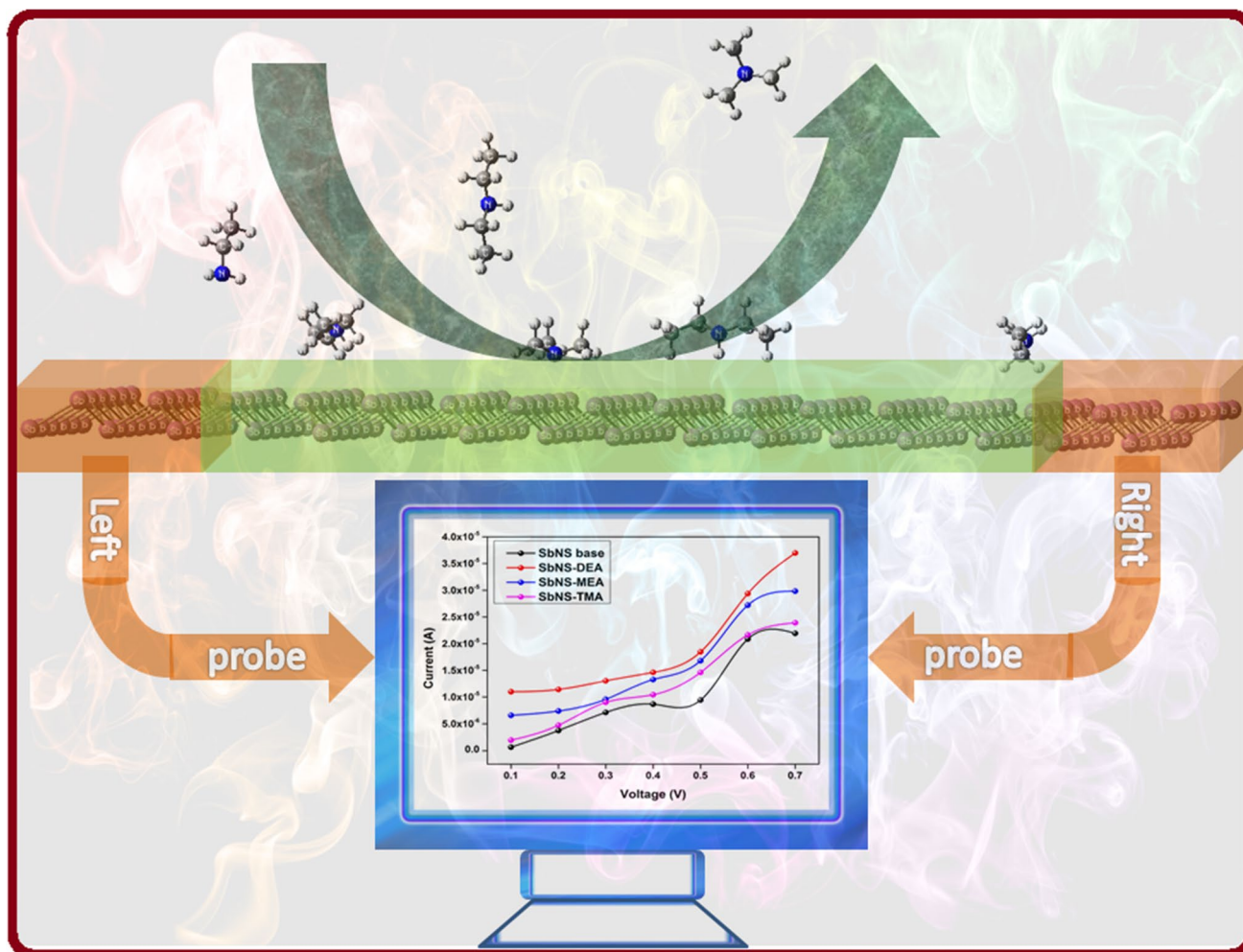
Abstract

The nonequilibrium Green's function and density functional theory methods are employed to investigate the electronic and adsorption properties of diethylamine (DEA), monoethylamine (MEA), and trimethylamine (TMA) organic molecules on an antimonene nanosheet (SbNS). The electron transitions between the organic molecules and the SbNS base material are examined based on the projected density-of-states spectrum and energy band structure. Furthermore, the electron transfer when the organic molecules are adsorbed onto the surface of SbNS is studied based on the bandgap energy, average energy gap variation, Bader charge transfer, and adsorption energy. The mixed physisorption–chemisorption of the organic molecules DEA, MEA, and TMA onto SbNS are explored based on the mentioned attributes. Moreover, the current–voltage (I – V) characteristics and the plot of the electron transitions confirm the utility of the SbNS base material to form a chemiresistive sensor for detecting reducing compounds such as DEA, MEA, and TMA in vapor form.

✉ R. Chandiramouli
rcmvgn@gmail.com

¹ School of Electrical and Electronics
Engineering, SASTRA Deemed University,
Tirumalaisamudram, Thanjavur 613 401, India

Graphical Abstract



Keywords Antimonene · Nanosheet · Band structure · Adsorption · Charge transfer

1 Introduction

One of the greatest breakthroughs in the field of planar two-dimensional (2D) materials was the discovery of graphene, a carbon allotrope. The electronic features of graphene, including high carrier mobility, massless Dirac fermions, high lattice thermal conductivity, etc., have fascinated many scientists and motivated them to explore this favorable material. However, the absence of a bandgap in graphene limits the application of this material in the field of nanoelectronics. Today, the bandgap is a primary criterion for nanomaterials, due to its effects on their electronic properties. This has resulted in the search for new 2D nanomaterials with a bandgap, yielding nanomaterials with a bandgap including boron nitride, MoS₂, silicene, phosphorene, germanene, arsenene, antimonene, etc. [1]. Antimonene is a 2D material

formed from a single layer of Sb atoms, attracting attention from researchers due to its optimum stability and ample bandgap. The bandgap of antimonene is estimated to be 2.28 eV. Based on a survey of literature, it is observed that Raman spectroscopy and transmission electron microscopy have been employed to verify the buckled graphene-like configuration of antimonene [2, 3]. Based on theoretical computations, it is predicted that an antimonene monolayer can exist in two different phases, viz. α -antimonene with a puckered structure and β -antimonene with a buckled structure [4]. Comparison of these two allotropes reveals that the bandgap of β -antimonene is greater. Also, note that the band-edge states in antimonene are chiefly of p_{xy} and s types. Moreover, owing to its semiconducting nature, antimonene exhibits fewer vacancies [5]. The outstanding properties of antimonene that have fascinated the scientific

community include its strain-induced band transition [6], i.e., the transformation from an indirect- to direct-bandgap semiconductor when biaxial strain is applied [7], excellent thermal conductivity [7], spintronic response [8], and outstanding carrier mobility [9]. It has been discovered that the lattice thermal conductivity can be decreased by chemical functionalization [10]. Also, compared with graphene and phosphorene, the atomic radius of Sb has little impact on the lattice configuration. Studies on the fabrication of 2D antimonene monolayers have revealed the following effects: The excellent stability of the buckled antimonene nanostructure and the variation of the bandgap from the bulk (semimetal) to monolayer (semiconductor) form were reported by Zhang et al. [11]. Using the electrochemical exfoliation method, the optical response and stable nature of multilayered antimonene were analyzed by Lu et al. [12]. The effects of the size and edges on the thermal conductivity of the two phases of antimonene mentioned above (α and β) were examined by Gupta et al. [13]. In addition to the discovery of α - and β -antimonene, two other forms of antimonene, namely γ and δ , were identified and their geometrical properties investigated theoretically by Wang et al. [7]. Furthermore, the stability of all four allotropes (α -, β -, γ -, and δ -Sb) was investigated based on phonon dispersion calculations in a previous article. The existence of phosphorene nanotubes, nanoribbons, and van der Waals multilayers was suggested by Guo et al. [14] based on first-principle studies. With the aid of van der Waals epitaxial growth, Ji et al. [2] reported a single 2D antimonene crystal. It has been reported that the weak interactions between the layers in antimonene enable the use of techniques such as liquid-phase exfoliation and micromechanical cleavage to scale off single layers from multilayer antimonene [2]. Moreover, the mechanical exfoliation method has also been utilized to synthesize antimonene flakes [3]. Also, antimonene was fabricated by molecular beam epitaxy on Ag (1 1 1) by Mao et al. [15], and Sb_2Te_3 and Bi_2Te_3 by Lei et al. [16]. Moreover, due to its stability, the buckled honeycomb structure is synthesized when depositing Sb onto the surface of AgSb_2 alloy. In particular, the fabrication of nanodevices requires such formation of antimonene on a substrate. In this regard, the dependence of antimonene formation on the surface energy was reported [7]. The use of antimonene and other group V nanomaterials in the fields of chemical sensors and nanoelectronic devices was initially envisaged by the group of Haibo Zeng [17–20] as a result of their extended research on the electronic properties of antimonene [20]. In addition, the group of Ullah has also extensively studied the binding properties of gas molecules onto various polymers as well as the corresponding electronic properties [21–31].

Volatile organic compounds such as diethylamine (DEA), monoethylamine (MEA), and trimethylamine (TMA) can be adsorbed onto a antimonene nanosheet (SbNS), which

is therefore suggested as a base substrate for their detection in the present research. Diethylamine (DEA) is a flammable secondary amine, being colorless in nature with formula $(\text{CH}_3\text{CH}_2)_2\text{NH}$. It is an alkaline liquid with an intense ammonia-like odor. The National Institute for Occupational Safety and Health (NIOSH) has determined permissible exposure limits with a recommended exposure limit of 25 ppm (75 mg/m^3) and 10 ppm (30 mg/m^3) time-weighted average (TWA). Even though DEA is less poisonous, its vapor results in temporary vision damage. Monoethylamine (MEA) is a lucid, achromatic liquid with potent (ammonia-like) odor, having formula $\text{CH}_3\text{CH}_2\text{NH}_2$. The NIOSH and Occupational Safety and Health Administration (OSHA) have fixed exposure level limits of 10 ppm TWA (18 mg/m^3). It leads to skin burns, dermatitis, damage to the respiratory system, and eye and skin irritation. On the other hand, trimethylamine (TMA) $[(\text{CH}_3)_3\text{N}]$ is a flammable, hygroscopic tertiary amine, which is in the gaseous phase at 273 K, but also present in the form of 40% solution in water. It has an ammonia-like odor at higher concentrations but a potent fish-like odor at lower concentrations. The recommended exposure limit is set at 10 ppm TWA (24 mg/m^3) by the NIOSH. The chief objective of the current work is to explore the surface adsorption properties of DEA, MEA, and TMA on SbNS along with its electronic properties, thereby facilitating the use of SbNS in chemosensors.

2 Computational details

The geometric structure of the antimonene nanosheet (SbNS) is interpreted to study its surface adsorption properties for the organic molecules diethylamine (DEA), monoethylamine (MEA), and trimethylamine (TMA) in addition to the electronic properties of the SbNS base material with the help of the nonequilibrium Green's function (NEGF) method and density functional theory (DFT). The entire process is carried out using the SIESTA package, more specifically in the TranSIESTA module [32]. The supercell of SbNS consists of 192 Sb atoms, and its ideal structure is obtained when using $20 \times 20 \times 1$ sampling in the Brillouin zone and decreasing the atomic forces on the Sb atoms to below 0.01 eV/\AA . To investigate the interaction between the electrons and optimize the local structure, the van der Waals density functional (vdW-DF) dispersion correction [33] is included along with the generalized gradient approximation (GGA) and the Perdew–Burke–Ernzerhof (PBE) exchange–correlation functional for the SbNS base material [34, 35]. Moreover, when optimizing the structure of SbNS, the double zeta polarization (DZP) basis set is applied [36, 37]. Also, the atoms in SbNS are allowed to move freely until convergence is achieved with forces below 0.01 eV/\AA .

Furthermore, the additional response of the SbNS base material when the organic molecules DEA, MEA, and TMA are surface adsorbed is investigated. In addition, overlap of periodic images of SbNS is avoided by using vacuum padding of 18 Å along the x - and y -axes.

3 Results and discussion

3.1 The structure and electronic properties of the antimonene nanosheet

Antimony atoms constitute the entire antimonene nanosheet, which is separated into three sections for computation purposes, called the left electrode, right electrode, and center scattering region, where a voltage of 0.1–0.7 V is applied. The stability of a perfect antimonene nanosheet can be investigated based on its energy of formation [38, 39], computed using the expression

$$E_{\text{form}} = (1/x) [E(\text{SbNS}) - xE(\text{Sb})].$$

Based on this equation, the energy of formation is estimated to be -4.420 eV. This negative value of the energy of formation confirms the stability of the base material. Figure 1a shows a schematic of the isolated antimonene nanosheet molecular device.

In this work, the use of such an antimonene nanosheet (SbNS) for the detection of diethylamine (DEA), monoethylamine (MEA) and trimethylamine (TMA), three important molecules in the field of organic chemistry, is investigated. Figure 1b–d depicts the adsorption of DEA, MEA, and TMA molecules onto SbNS in various configurations A, B, and C, respectively.

The adsorption behavior of DEA, MEA, and TMA organic molecules onto SbNS is investigated based on various electronic properties. Moreover, the DEA, MEA, and TMA molecules exhibit mixed (physisorption and chemisorption) type of adsorption onto SbNS. The variation of the current on application of a voltage bias is measured as a function of the concentration of DEA, MEA, or TMA molecules.

3.2 The electronic properties of the antimonene nanosheet

The main aim of the current work is to explore the surface adsorption properties of an antimonene nanosheet (SbNS) for DEA, MEA, and TMA molecules along with the electronic features of the SbNS nanomaterial. The energy band structure and density-of-states (DOS) spectrum of the isolated SbNS are depicted in Fig. 2a. Moreover, the energy band structure and projected density of states (PDOS) spectrum for SbNS with DEA, MEA, and TMA molecules

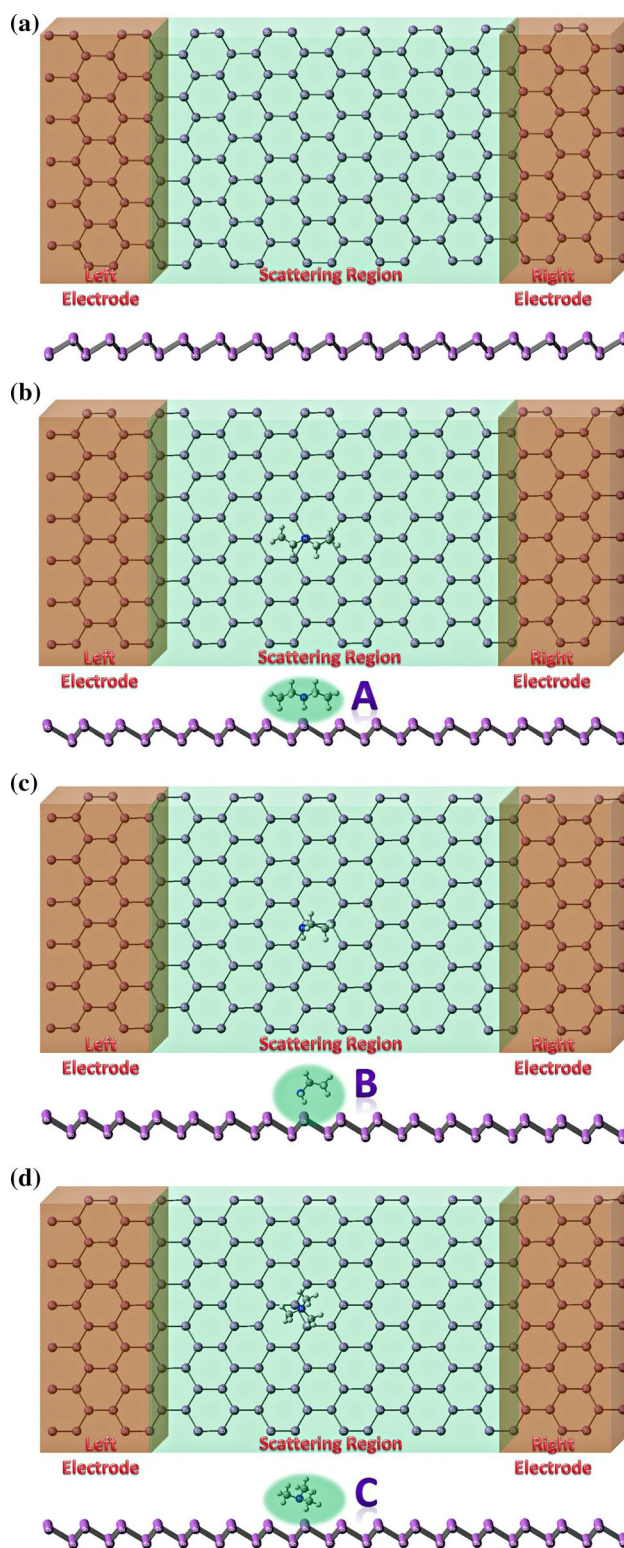
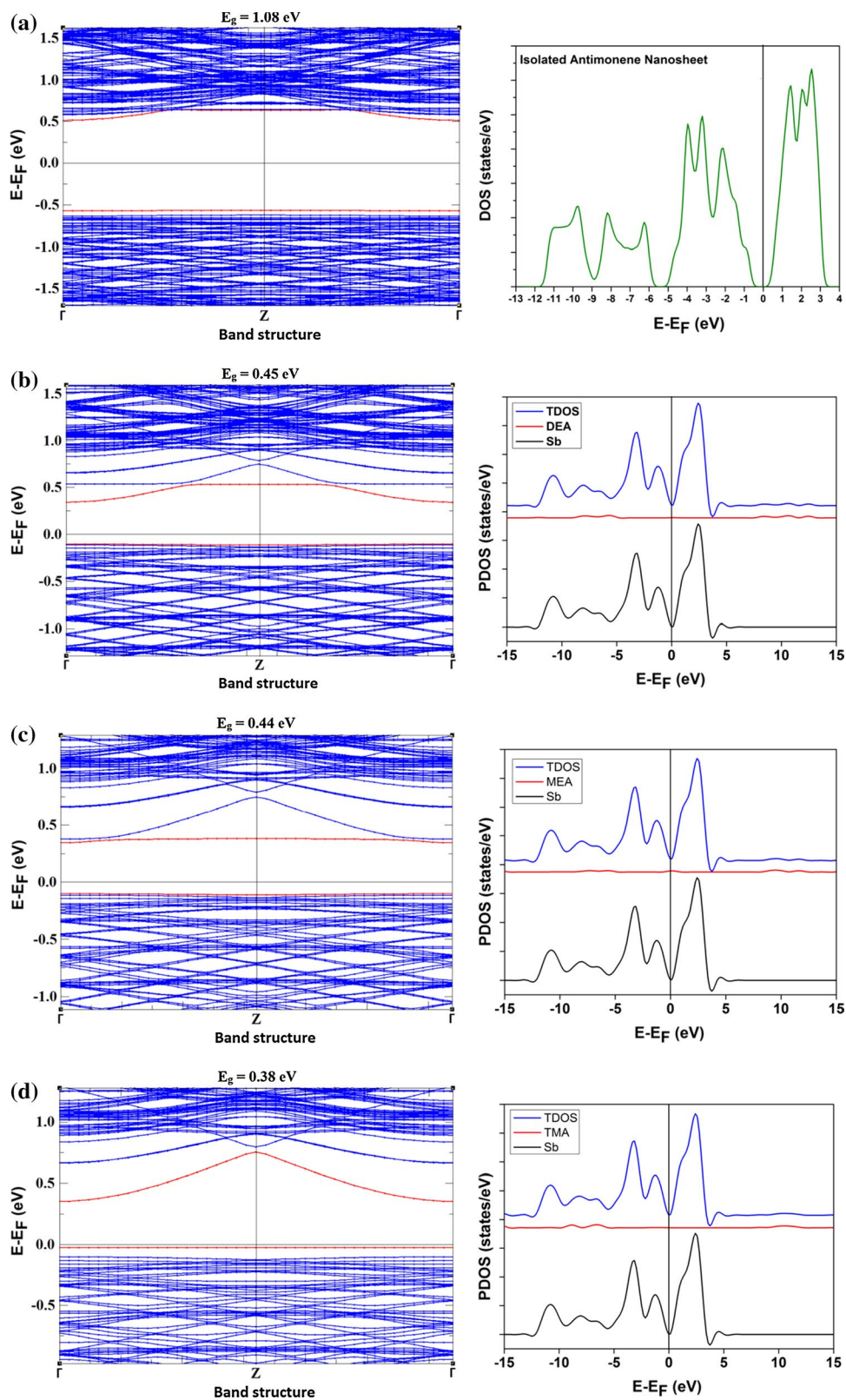


Fig. 1 a The isolated antimonene nanosheet (SbNS) molecular device. b The interaction of diethylamine on the SbNS nanosheet in orientation A. c The interaction of monoethylamine on the SbNS nanosheet in orientation B. d The interaction of trimethylamine on the SbNS nanosheet in orientation C

Fig. 2 **a** A pictorial representation of the band structure and density of states (DOS) of isolated SbNS. **b** The projected density of states (PDOS) and band structure for orientation A. **c** The PDOS and band structure for orientation B. **d** The PDOS and band structure for orientation C



adsorbed in orientation A, B, and C are illustrated in Fig. 2b, c, and d, respectively. The estimated bandgap of the isolated SbNS is 1.08 eV at the Γ point.

When the organic molecules DEA, MEA, and TMA are adsorbed onto the surface of SbNS, the bandgap shifts to 0.45 eV, 0.44 eV, and 0.38 eV, correspondingly.

The PDOS spectrum throws light on the dispersion of the various levels as a function of energy [40–44]. From the PDOS spectrum, it is evident that the peaks are shifted in various energy intervals compared with SbNS alone. Electron transfer between the SbNS and the organic molecules is confirmed by the observation of a maximum peak adjacent to the Fermi energy level (E_F). Furthermore, the interaction of electrons among the antimonene atoms of SbNS affects the maximum peak observed in different energy intervals. This natural transfer of electrons between the organic molecules and SbNS indicates the chemiresistive nature of the SbNS base material. Moreover, a change in the DOS spectrum of SbNS is observed upon surface adsorption of the organic molecules DEA, MEA, and TMA. Thus, it is deduced from the PDOS spectrum and energy band structure that SbNS could indeed be employed in the assembly of chemiresistive sensors.

3.3 The adsorption of DEA, MEA, and TMA onto the surface of SbNS

The adsorption energy E_{ads} can be calculated using the energy of the isolated SbNS, the energy of the organic molecules (DEA, MEA, and TMA individually), and the combined energy of SbNS with the adsorbed organic molecules [45–49]. (Refer to our previous article for this calculation of the adsorption energy.)

Moreover, the important parameters determining the sensing ability of the SbNS base material are the adsorption energy (E_{ads}), the energy bandgap (E_g), the average energy bandgap (E_g^a), and the Bader charge transfer (Q), as specified in Table 1.

From the estimated adsorption energies for orientation A, B, and C (i.e., SbNS-DEA, SbNS-MEA, and SbNS-TMA), it is seen that the DEA molecule will show the maximum adsorption onto SbNS owing to its high magnitude of -3.089 eV compared with MEA (-1.855 eV) or TMA (-2.474 eV). Interestingly, the adsorption energies are overestimated when the vdW-DF dispersion correction is included in the calculation. However, only slight variation is observed in the vdW-DF-corrected E_{ad} , in the range from 0.038 to 0.154 eV. Moreover, the negative value also indicates an enhanced adsorption ability of the organic

molecules [50]. The high value of the adsorption energy for orientation A is attributed to the fact that DEA exhibits a strong positive inductive ($+I$) effect. Compared with the other organic molecules, the presence of two ethyl (electron-donating) groups along with its less electronegative nature enhances the effective adsorption of DEA onto SbNS (orientation A). The next parameter determining the detection capability of SbNS is the energy bandgap (E_g), which is reduced upon the adsorption of DEA, MEA, and TMA molecules [51–54]. The bandgap of 1.08 eV for the isolated SbNS decreases to 0.45 eV, 0.44 eV, and 0.38 eV for the configurations A (DEA), B (MEA), and C (TMA). A strong decrease in the bandgap is observed on surface adsorption of the organic molecules onto SbNS. Comparing the bandgaps for orientation A (DEA) and B (MEA), the apparent slight variation (by 0.01 eV) can be easily explained by the fact that the two organic molecules contain ethylamine. However, the type of organic molecule is determined by the number of ethylamine groups present, i.e., two for DEA and one for MEA. Also, note that both of these organic molecules are obtained as byproducts in the synthesis of ethylamine. These reasons validate the slight change in the bandgap between orientation A and B. However, the scenario is different in the case of orientation C (TMA). It is well known that steric hindrance/resistance, i.e., the ability to slow down chemical reactions, increases with increasing number of alkyl groups. Therefore, when comparing the organic molecules studied herein (DEA, MEA, and TMA), TMA has the least alkyl groups and thus a low hindrance effect, resulting in a narrower bandgap compared with the other two molecules. The reduction in the bandgap can be justified by the fact that DEA, MEA, and TMA are reducing vapors. This reduction in the bandgap, in turn, leads to an increase in the current conduction, i.e., the conductivity of the SbNS. One question that emerges is why the bandgap decreases upon surface adsorption of the organic molecules DEA, MEA, and TMA onto SbNS? The reason behind this effect is that the investigated vapors are of reducing type, thus the lowest unoccupied molecular orbital (LUMO) and highest occupied molecular orbital (HOMO) are altered by the interaction between the SbNS and organic molecules. The sensing ability of the SbNS is then based on the resulting effect on E_g .

Table 1 The most important parameters determining the surface adsorption behavior of the target vapors onto SbNS

Nanostructure	Adsorption energy, E_{ad} (eV)	vdW-DF corrected adsorption energy, E_{ad} (eV)	Bader charge transfer, Q (e)	Bandgap, E_g (eV)	Average band-gap change, E_g^a %
SbNS base	–	–	–	1.08	–
Orientation A	-3.089	-3.127	0.290	0.45	58.33
Orientation B	-1.855	-2.009	0.217	0.44	59.26
Orientation C	-2.474	-2.612	0.219	0.38	64.81

The bandgap structure can also be used to investigate the surface adsorption properties of the organic molecules DEA, MEA, and TMA onto SbNS [55, 56]. Comparison of the DOS spectrum of the isolated SbNS and organic molecules adsorbed SbNS reveals that the number of available electron states reduces upon adsorption of the organic molecules in various energy intervals, implying electron transitions between the SbNS base material and the organic molecules. Moreover, the precise peak maxima observed in both the valence and conduction bands for the orientation A, B, and C with a decreased number of peaks also indicate electron transfer between the organic molecules and the SbNS base material.

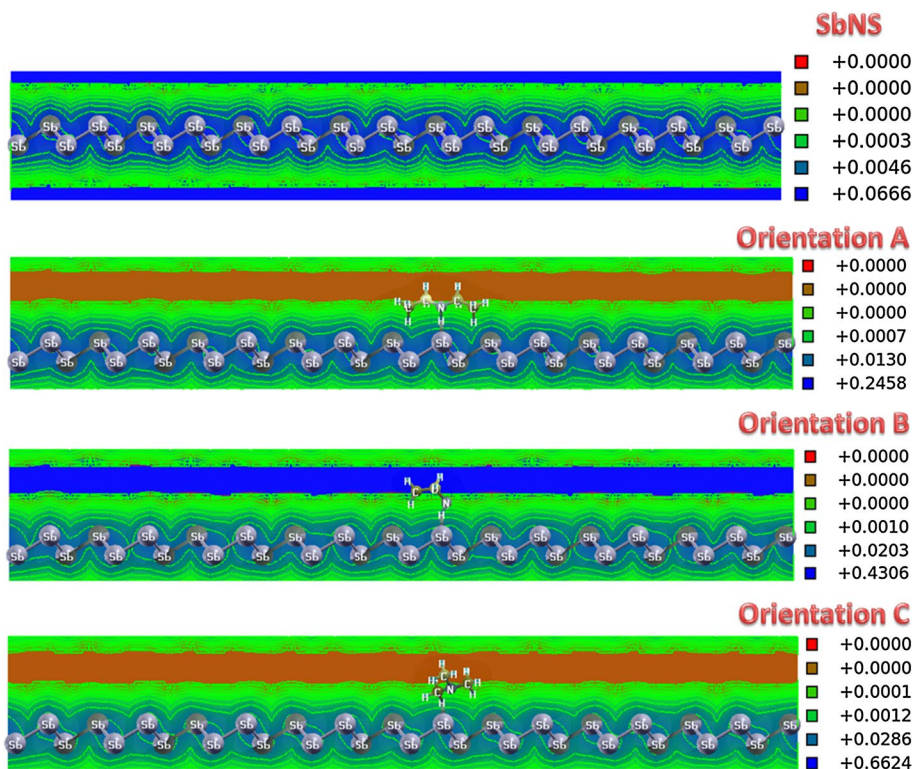
To explore the adsorption of DEA, MEA, and TMA onto the surface of the SbNS base material at the atomistic level, the Bader charge transfer (Q) and average energy gap variation (E_g^a %) for both the isolated material and organic molecules adsorbed material are ascertained. The most important adsorption site for the organic molecules can be determined using the average energy gap variation [57–61]. Based on the estimated values, it is observed that adsorption of the organic molecule TMA (64.81%) onto SbNS results in a significant variation of E_g^a , followed by MEA and DEA with values of 59.26% and 58.33%, respectively. The Bader charge transfer (Q) can be utilized to study the electron transfer taking place between the SbNS and the organic molecules. Based on the sign of Q , the characteristics of the vapor molecules and the kind of base material can be resolved. The computed values

are $0.290e$, $0.217e$, and $0.219e$ for configurations A, B, and C, respectively; these positive values indicate charge transfer from the organic molecules to SbNS. Upon adsorption of amine vapor onto the SbNS base material, electron transfer takes place from amine molecules towards SbNS, according to the Bader charge transfer results. These results show that SbNS acts as an electron-withdrawing material, leading to a change in the current flowing through the molecular device after adsorption of the vapor molecules. In addition, to validate the occurrence of charge transfer between the SbNS and target molecules, the electron density before and after adsorption of the organic molecules onto SbNS is calculated. Figure 3 shows the electron density of the pristine SbNS material and volatile organic molecules adsorbed SbNS material. The observed change in the electron density in SbNS after adsorption of the target molecules confirms the charge transfer towards SbNS.

3.4 The transmission characteristics of SbNS after adsorption of DEA, MEA, and TMA

The transmission spectrum provides further support for the electronic properties of SbNS and after surface adsorption of the DEA, MEA, and TMA molecules. The transmission $T(E, V)$ spectrum is obtained based on the following formula involving the coupling function, and the advanced and retarded Green’s functions [62, 63]. (Refer to our previous article for this expression.) [64]. Owing to the delocalization

Fig. 3 The electron density of pristine SbNS and after adsorption of the volatile organic molecules



of the orbits adjacent to the Fermi energy level, the rate of electron flow along the SbNS is increased, as revealed by the particular peak voltages in the transmission spectrum of SbNS. The transmission spectrum is plotted in three dimensions for the isolated SbNS and after adsorption of the organic molecules (DEA, MEA, and TMA) in Fig. 4a–d for bias voltages in the range of 0.1–0.7 V.

The peak maximum is found along the conduction band for the isolated SbNS, indicating the chemosensing nature of the base material. Upon surface adsorption of the organic molecules, a shift in the peak is observed for distinct energy levels. For orientation A, more peaks are found in the valence band, indicating a steady transfer of electrons between the DEA and the SbNS base material. However, a moderate number of peaks are found in the valence band for

orientation B (SbNS—MEA) when compared with adsorption of DEA, showing that the organic molecule MEA follows DEA in terms of adsorption onto SbNS. The peaks are distributed in both the valence and conduction band for orientation C, i.e., for adsorption of TMA. However, compared with the conduction band, more peaks are found in the valence band, confirming the electron transfer between the TMA and SbNS and that the organic molecule TMA is in third place in terms of adsorption onto SbNS. These results for the transmission spectra clearly confirm the transfer of charge between the SbNS and the organic molecules. This electron transfer between the materials significantly enhances the current conduction in the SbNS base material. As mentioned above, the reducing behavior of the organic molecules also influences (to be precise, increases) the

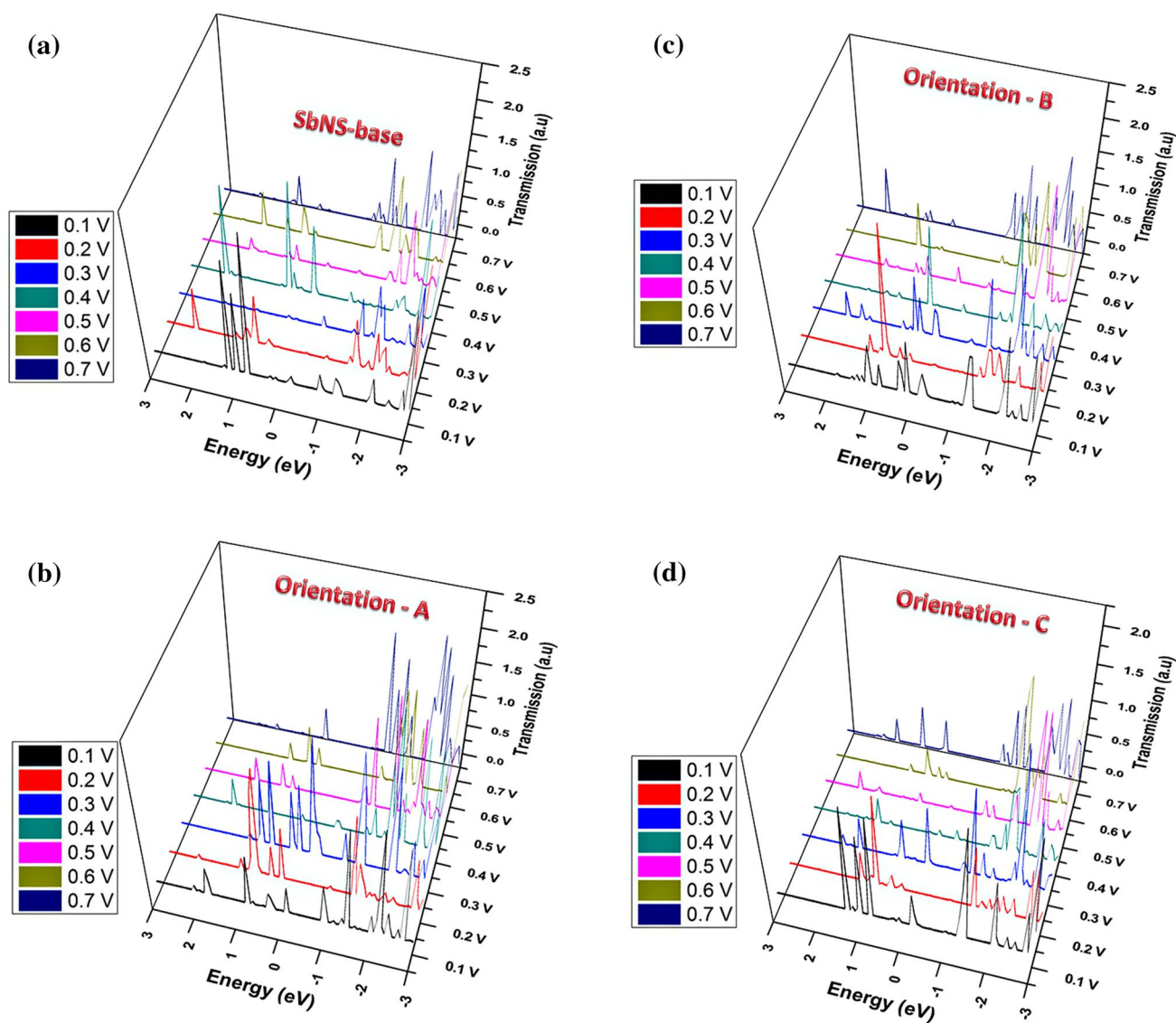


Fig. 4 **a** The transmission spectrum of the isolated SbNS nanosheet. **b** The transmission spectrum for orientation A. **c** The transmission spectrum for orientation B. **d** The transmission spectrum for orientation C

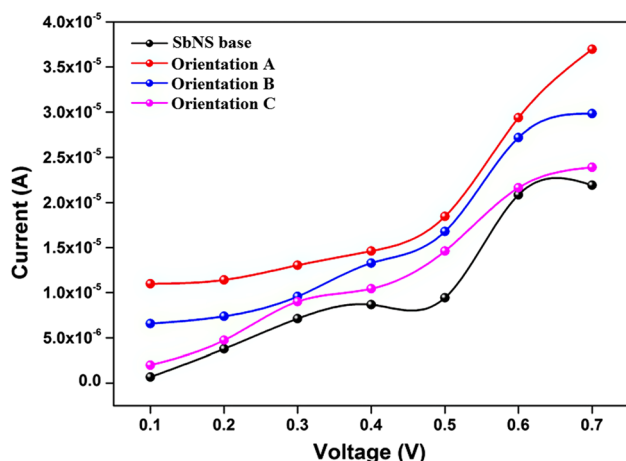


Fig. 5 The I – V characteristics of the pristine SbNS device and after adsorption of each target volatile compound

current conduction by decreasing the base resistance of the SbNS. The resulting increase in the current flow is measured using a two-probe method. Hence, the transmission spectrum results provide further evidence for the chemosensing nature of the SbNS, indicating the feasibility of SbNS-based sensing of DEA, MEA, and TMA.

3.5 The current–voltage characteristics of the SbNS device after adsorption of DEA, MEA, and TMA

The surface adsorption properties of DEA, MEA, and TMA molecules onto the SbNS molecular device is further investigated based on the I – V (current–voltage) characteristics [65, 66]. The current flow through the base material is explored with the help of the Landauer–Büttiker formula [67]. (Refer to our previous article.) [68]. The variation in the current flow upon adsorption of the organic molecules onto SbNS is measured in a two-probe chemiresistor configuration. The desorption or adsorption of the target gas/organic molecule and the resistance of the base material are related in a chemiresistive-type vapor/gas sensor. Thus, the variation in the resistance of the SbNS-based chemosensor is computed based on the change in the current conduction [69]. In addition, there is a linear relationship between the concentration of the adsorbed target vapor/gas molecules and the current conduction along the SbNS molecular device. Figure 5 presents the I – V characteristics of the isolated SbNS molecular device and after adsorption of each organic molecule.

As stated above, the nonoxidizing nature of the organic molecules DEA, MEA, and TMA leads to an increase in the

current flow along the SbNS molecular device. Moreover, based on this figure, it is apparent that the magnitude of the current is remarkably high for orientation A (i.e., SbNS–DEA), followed by orientation B (SbNS–MEA) and C (SbNS–TMA). Figure 6 provides insight into the interaction of the aforementioned organic molecules with the SbNS device.

The magnitude of the current for the isolated SbNS is found to be the least among the investigated systems. The variation in the current coincides with the statement above regarding the transmission spectra, i.e., electron transfer between the SbNS and organic molecules. The variation in the current is seen to be almost linear in the voltage bias range of 0.1–0.7 V. Hence, it can be inferred that the SbNS molecular device could be employed for detection of DEA, MEA, and TMA when operated in the range of 0.1–0.7 V.

4 Conclusions and future outlook

We have applied the DFT and NEGF methods to examine the surface adsorption properties of the organic molecules DEA, MEA, and TMA onto SbNS, along with the electronic features of the SbNS base material. The bandgap of the isolated SbNS is estimated to be 1.08 eV, and a maximum peak adjacent to the Fermi energy level is observed in the DOS spectrum, indicating the semiconducting nature of the SbNS. Also, computations of the adsorption energy, average energy gap variation, energy bandgap, and Bader charge transfer confirm the surface adsorption of DEA, MEA, and TMA onto SbNS. The electron transfer between the organic molecules and SbNS is visualized based on the energy band structure and DOS spectrum. Moreover, the transmission spectra reveal a shift in the peaks in various energy intervals, further illustrating the adsorption of the organic molecules onto SbNS. In addition, the electron transfer giving rise to current conduction is enhanced when the organic molecules adsorbed onto the surface of the base material, as further verified by the I – V characteristics, where the magnitude of the current is found to follow a linear relationship with the bias voltage (in the operating voltage range of 0.1–0.7 V for the SbNS chemiresistive sensor). Furthermore, the increase in the current flow on adsorption of the organic molecules onto the SbNS leads to a decrease in the base resistance. The results of the current calculations therefore robustly confirm the feasibility of using an antimonene nanosheet base material to develop chemiresistive molecular devices for detecting reducing compounds such as DEA, MEA, and TMA in vapor form.

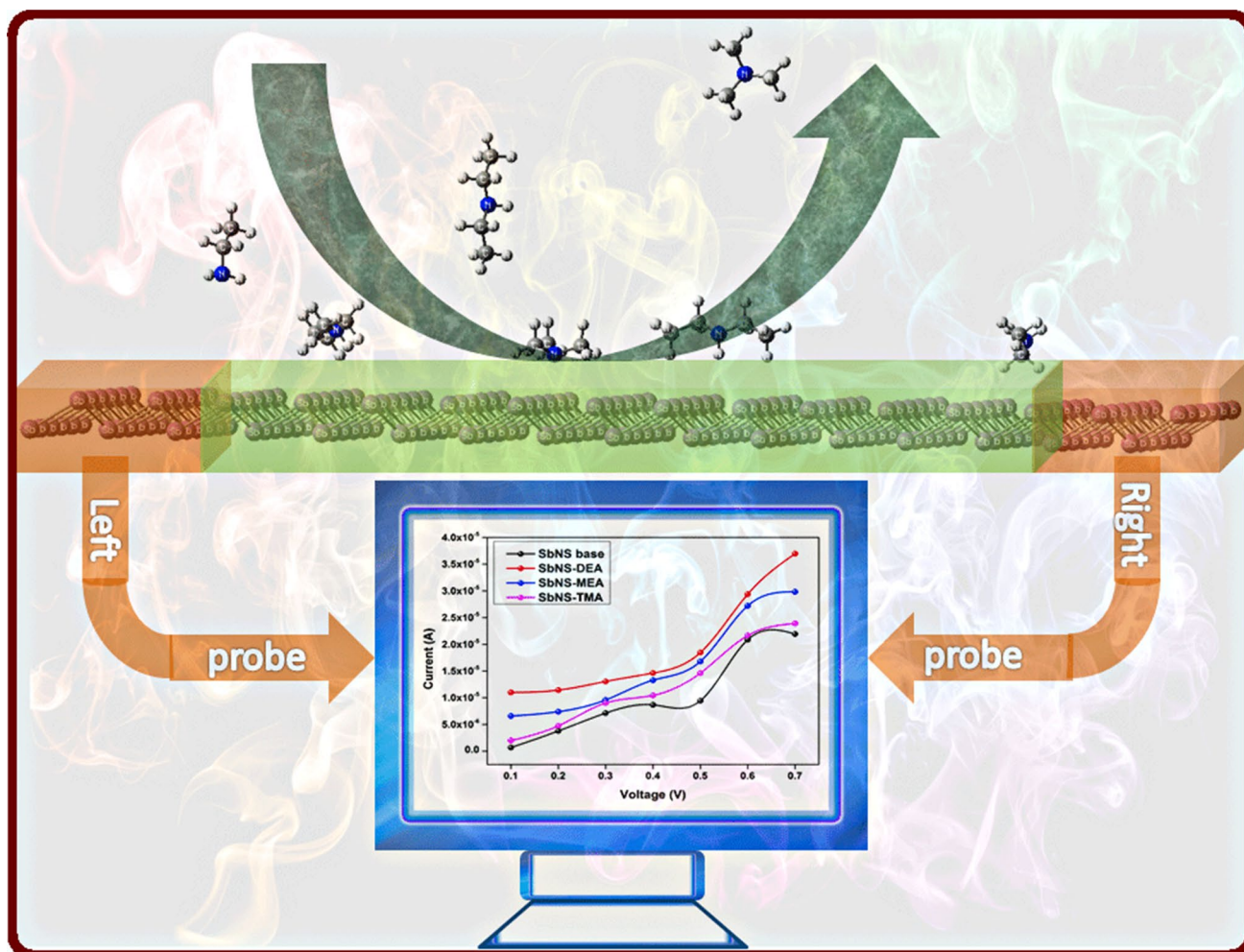


Fig. 6 A schematic showing the adsorption behavior of the target vapors onto the SbNS device

Acknowledgements The authors wish to express their sincere thanks to Nano Mission Council [no. SR/NM/NS-1011/2017(G)], Department of Science and Technology, India for financial support.

References

- Jin, S., Il, C., Kim, D.: Recent developments in 2D nanomaterials for chemiresistive-type gas sensors. *Electron. Mater. Lett.* **14**, 221–260 (2018)
- Ji, J., Song, X., Liu, J., Yan, Z., Huo, C., Zhang, S., Su, M., Liao, L., Wang, W., Ni, Z., Hao, Y., Zeng, H.: Two-dimensional antimonene single crystals grown by van der Waals epitaxy. *Nat. Commun.* **7**, 13352 (2016)
- Aldave, D.A., Zamora, F., Gómez-Herrero, J., Aguilar-Galindo, F., Ares, P., Alcamí, M., Rodríguez-San-Miguel, D., Díaz-Tendero, S., Martín, F.: Mechanical isolation of highly stable antimonene under ambient conditions. *Adv. Mater.* **28**, 6332–6336 (2016)
- Zhang, F., Wang, M., Wang, Z., Han, K., Liu, X., Xu, X.: Excellent nonlinear absorption properties of β -antimonene nanosheets. *J. Mater. Chem. C* **6**, 2848–2853 (2018)
- Liu, Y., Xu, F., Zhang, Z., Penev, E.S., Yakobson, B.I.: Two-dimensional mono-elemental semiconductor with electronically inactive defects: the case of phosphorus. *Nano Lett.* **14**, 6782–6786 (2014)
- Zhao, M., Zhang, X., Li, L.: Strain-driven band inversion and topological aspects in antimonene. *Sci. Rep.* **5**, 16108 (2015)
- Wang, G., Pandey, R., Karna, S.P.: Atomically thin group V elemental films: theoretical investigations of antimonene allotropes. *ACS Appl. Mater. Interfaces* **7**, 11490–11496 (2015)
- Lee, J., Tian, W., Wang, W., Yao, D.: Two-dimensional pnictogen honeycomb lattice: structure, on-site spin-orbit coupling and spin polarization. *Sci. Rep.* **5**, 11512 (2015)
- Zhang, S., Xie, M., Li, F., Yan, Z., Li, Y., Kan, E., Liu, W., Chen, Z., Zeng, H.: Semiconducting group 15 monolayers: a broad range of band gaps and high carrier mobilities. *Angew. Chem.* **128**, 1698–1701 (2016)
- Zhang, T., Qi, Y.-Y., Chen, X.-R., Cai, L.-C.: Predicted low thermal conductivities in antimony films and the role of chemical functionalization. *Phys. Chem. Chem. Phys.* **18**, 30061–30067 (2016)
- Zhang, S., Yan, Z., Li, Y., Chen, Z., Zeng, H.: Atomically thin arsenene and antimonene: semimetal–semiconductor and

- indirect–direct band-gap transitions. *Angew. Chem. Int. Ed.* **54**, 1–5 (2015)
12. Lu, L., Tang, X., Cao, R., Wu, L., Li, Z., Jing, G., Dong, B., Lu, S., Li, Y., Xiang, Y., Li, J., Fan, D., Zhang, H.: Broadband nonlinear optical response in few-layer antimonene and antimonene quantum dots: a promising optical Kerr media with enhanced stability. *Adv. Opt. Mater.* **5**, 1700301 (2017)
 13. Gupta, S.K., Sonvane, Y., Wang, G., Pandey, R.: Size and edge roughness effects on thermal conductivity of pristine antimonene allotropes. *Chem. Phys. Lett.* **641**, 169–172 (2015)
 14. Guo, H., Lu, N., Dai, J., Wu, X., Zeng, X.C.: Phosphorene nanoribbons, phosphorus nanotubes, and van der Waals multilayers. *J. Phys. Chem. C* **118**, 14051–14059 (2014)
 15. Mao, Y., Zhang, L., Wang, H., Shan, H., Zhai, X., Hu, Z., Zhao, A., Wang, B.: Epitaxial growth of highly strained antimonene on Ag (111). *Front. Phys.* **13**, 138106 (2018)
 16. Wu, R., Li, Y.-P., Wang, H.-Q., Li, J.-M., Lei, T., Liu, C., Ibrahim, K., Zhao, J.-L., Wang, J.-O., Qian, H.-J.: Electronic structure of antimonene grown on Sb_2Te_3 (111) and Bi_2Te_3 substrates. *J. Appl. Phys.* **119**, 015302 (2016)
 17. Huang, Y., Zhu, C., Zhang, S., Hu, X., Zhang, K., Zhou, W., Guo, S., Xu, F., Zeng, H.: Ultrathin bismuth nanosheets for stable Na-Ion batteries: clarification of structure and phase transition by in situ observation. *Nano Lett.* **19**, 1118–1123 (2019)
 18. Xie, M., Zhang, S., Cai, B., Gu, Y., Liu, X., Kan, E., Zeng, H.: Van der Waals bilayer antimonene: a promising thermophotovoltaic cell material with 31% energy conversion efficiency. *Nano Energy* **38**, 561–568 (2017)
 19. Ji, J., Zhang, S., Chen, Z., Zeng, H., Zhu, Z., Ma, Y., Cai, B., Yang, S.A., Zhou, W.: Antimonene oxides: emerging tunable direct bandgap semiconductor and novel topological insulator. *Nano Lett.* **17**, 3434–3440 (2017)
 20. Zhang, S., Guo, S., Chen, Z., Wang, Y., Gao, H., Gómez-Herrero, J., Ares, P., Zamora, F., Zhu, Z., Zeng, H.: Recent progress in 2D group-VA semiconductors: from theory to experiment. *Chem. Soc. Rev.* **47**, 982–1021 (2018)
 21. Ullah, H., Shah, A.A., Bilal, S., Ayub, K.: DFT study of polyaniline NH_3 , CO_2 , and CO gas sensors: comparison with recent experimental data. *J. Phys. Chem. C* **117**, 23701–23711 (2013)
 22. Bibi, S., Ullah, H., Ahmad, S.M., Ali Shah, A.-H., Bilal, S., Tahir, A.A., Ayub, K.: Molecular and electronic structure elucidation of polypyrrole gas sensors. *J. Phys. Chem. C* **119**, 15994–16003 (2015)
 23. Ullah, H., Ayub, K., Ullah, Z., Hanif, M., Nawaz, R., Shah, A.U.H.A., Bilal, S.: Theoretical insight of polypyrrole ammonia gas sensor. *Synth. Met.* **172**, 14–20 (2013)
 24. Yaseen, M., Ullah, Z., Hassan, W., Fazl-i-Sattar, Ullah, H., Tahir, A.A., Rauf, A., Ayub, K., Ata-ur-Rahman, Tariq, M.: Density functional theory and phytochemical study of 8-hydroxyisodiospyrin. *J. Mol. Struct.* **1095**, 69–78 (2015)
 25. Ullah, H., Bibi, S., Tahir, A.A., Mallick, T.K.: Donor-acceptor polymer for the design of all-solid-state dye-sensitized solar cells. *J. Alloys Compd.* **696**, 914–922 (2017)
 26. Mat Teridi, M.A., Safaei, J., Soh, M.F., Tahir, A.A., WanIsahak, W.N.R., Ahmad Ludin, N., Ullah, H., Mohamed, N.A., Ibrahim, M.A., Mohamad Noh, M.F.: Enhanced photoelectrochemical performance of Z-scheme $\text{g-C}_3\text{N}_4/\text{BiVO}_4$ photocatalyst. *Appl. Catal. B Environ.* **234**, 296–310 (2018)
 27. Ullah, H., Rauf, A., Ullah, Z., Fazl-i-Sattar, Anwar, M., Shah, A.U.H.A., Uddin, G., Ayub, K.: Density functional theory and phytochemical study of Pistagremic acid. *Spectrochim. Acta Part A Mol. Biomol. Spectrosc.* **118**, 210–214 (2014)
 28. Ali Tahir, A., Ullah, H., Sudhagar, P., Mat Teridi, M.A., Devadoss, A., Sundaram, S.: The application of graphene and its derivatives to energy conversion, storage, and environmental and biosensing devices. *Chem. Rec.* **16**, 1591–1634 (2016)
 29. Bibi, S., Bilal, S., Ali Shah, A.U.H., Ullah, H.: Systematic analysis of poly(o-aminophenol) humidity sensors. *ACS Omega* **2**, 6380–6390 (2017)
 30. Ullah, H., Shah, A.A., Ayub, K., Bilal, S.: Density functional theory study of poly(o-phenylenediamine) oligomers. *J. Phys. Chem. C* **117**, 4069–4078 (2013)
 31. Ullah, H., Bibi, S., Tahir, A.A., Mallick, T.K.: Density functional theory study of selenium-substituted low-bandgap donor-acceptor-donor polymer. *J. Phys. Chem. C* **120**, 27200–27211 (2016)
 32. Soler, M., Artacho, E., Gale, J.D., Garc, A., Junquera, J., Ordej, P., Daniel, S.: The SIESTA method for ab initio order-N materials simulation. *J. Phys. Condens. Matter* **14**, 2745 (2002)
 33. Roman-Perez, G., Soler, J.M.: Efficient implementation of a van der Waals density functional: application to double-wall carbon nanotubes. *Phys. Rev. Lett.* **103**, 096102 (2009)
 34. Perdew, J., Burke, K., Wang, Y.: Generalized gradient approximation for the exchange-correlation hole of a many electron system. *Phys. Rev. B* **54**, 16533–16539 (1996)
 35. Perdew, J.P., Burke, K., Ernzerhof, M.: Generalized gradient approximation made simple. *Phys. Rev. B* **77**, 3865–3868 (1996)
 36. Snehha, P., Nagarajan, V., Chandiramouli, R.: Novel bismuthene nanotubes to detect NH_3 , NO_2 and PH_3 gas molecules—a first-principles insight. *Chem. Phys. Lett.* **712**, 102–111 (2018)
 37. Bhavadharani, R.K., Nagarajan, V., Chandiramouli, R.: Density functional study on the binding properties of nucleobases to stanene nanosheet. *Appl. Surf. Sci.* **462**, 831–839 (2018)
 38. Snehha, P., Nagarajan, V., Chandiramouli, R.: Doped aluminum nanocones as an efficient electron field emitter: a first-principles investigation. *Inorg. Chem. Commun.* **96**, 5–12 (2018)
 39. Nagarajan, V., Chandiramouli, R.: Interaction of volatile organic compounds (VOCs) emitted from banana on stanene nanosheet—a first-principles studies. *Struct. Chem.* **29**, 1321–1332 (2018)
 40. Shokuhi, A., Ayub, K.: Adsorption of thiophene on the surfaces of $\text{X}_{12}\text{Y}_{12}$ ($\text{X} = \text{Al, B}$, and $\text{Y} = \text{N, P}$) nanoclusters. A DFT study. *J. Mol. Liq.* **238**, 303–309 (2017)
 41. Kaloni, T.P., Gangopadhyay, S., Singh, N., Jones, B., Schwingschl, U.: Electronic properties of Mn-decorated silicene on hexagonal boron nitride. *Phys. Rev. B* **88**, 235418 (2013)
 42. Shokuhi, A., Mehdi, S., Poralijan, V., Peyravi, M., Mirzaei, M.: Application of pristine and Ni-decorated $\text{B}_{12}\text{P}_{12}$ nano-clusters as superior media for acetylene and ethylene adsorption: DFT calculations. *Comput. Theor. Chem.* **1109**, 1–9 (2017)
 43. Ullah, H., Tahir, A.A., Mallick, T.K.: Polypyrrole/ TiO_2 composites for the application of photocatalysis. *Sens. Actuators B* **241**, 1161–1169 (2017)
 44. Chandiramouli, R.: Antimonene nanosheet device for detection of explosive vapors—a first-principles inspection. *Chem. Phys. Lett.* **708**, 130–137 (2018)
 45. Rad, A.S., Abedini, E.: Chemisorption of NO on Pt-decorated graphene as modified nanostructure media: a first principles study. *Appl. Surf. Sci.* **360**, 1041–1046 (2016)
 46. Beheshtian, J., Soleymanabadi, H., Ahmadi, A., Bagheri, Z.: A DFT study on the functionalization of a BN nanosheet with PC X, ($\text{PC} = \text{phenyl carbamate}$, $\text{X} = \text{OCH}_3, \text{CH}_3, \text{NH}_2, \text{NO}_2$ and CN). *Appl. Surf. Sci.* **268**, 436–441 (2013)
 47. Samadzadeh, M., Rastegar, S.F., Peyghan, A.A.: The electronic response of nano-sized tube of BeO to CO molecule: a density functional study. *Struct. Chem.* **26**, 809–814 (2015)
 48. Beheshtian, J., Ahmadi, A., Noei, M.: Chemical sensing behavior of Al and Si doped BC_3 graphenes to formaldehyde. *Sens. Actuators B Chem.* **181**, 829–834 (2013)
 49. Nagarajan, V., Chandiramouli, R.: Novel method to detect the lung cancer biomarker volatiles using hydrogen vacant silicene nanosheets: a DFT investigation. *Comput. Theor. Chem.* **1138**, 107–116 (2018)

50. Dharani, S., Nagarajan, V., Chandiramouli, R.: Nucleobases adsorption studies on silicane layer: a first-principles investigation. *J. Mol. Graph. Model.* **85**, 48–55 (2018)
51. Ullah, H.: Inter-molecular interaction in polypyrrole/TiO₂: a DFT study. *J. Alloys Compd.* **692**, 140–148 (2017)
52. Beheshtian, J., Bagheri, Z., Kamfiroozi, M., Ahmadi, A.: Toxic CO detection by B₁₂N₁₂ nanocluster. *Microelectron. J.* **42**, 1400–1403 (2011)
53. Kaloni, T.P., Schreckenbach, G., Freund, M.S.: Large enhancement and tunable band gap in silicene by small organic molecule adsorption. *J. Phys. Chem. C* **118**, 23361–23367 (2014)
54. Bhuvanewari, R., Nagarajan, V., Chandiramouli, R.: First-principles insights on the electronic and field emission properties of Ga and Al doped germanium nanocones. *J. Electron Spectros. Relat. Phenom.* **227**, 15–22 (2018)
55. Kaloni, T.P., Schwingenschlögl, U.: Stability of germanene under tensile strain. *Chem. Phys. Lett.* **583**, 137–140 (2013)
56. Bhuvanewari, R., Nagarajan, V., Chandiramouli, R.: Arsenene nanotube as a chemical sensor to detect the presence of explosive vapors: a first-principles insight. *J. Inorg. Organomet. Polym.* **28**, 2844 (2018)
57. Srimathi, U., Nagarajan, V., Chandiramouli, R.: Interaction of Imuran, Pentasa and Hyoscyamine drugs and solvent effects on graphdiyne nanotube as a drug delivery system—a DFT study. *J. Mol. Liq.* **265**, 199–207 (2018)
58. Bhuvanewari, R., Chandiramouli, R.: DFT investigation on the adsorption behavior of dimethyl and trimethyl amine molecules on borophene nanotube. *Chem. Phys. Lett.* **701**, 34–42 (2018)
59. Ahmadi, A., Somayeh, P.: Selective detection of F₂ in the presence of CO, N₂, O₂, and H₂ molecules using a ZnO nanocluster. *Monatsh. Chem.* **146**, 1233–1239 (2015)
60. Nagarajan, V., Chandiramouli, R.: Adsorption behavior of NH₃ and NO₂ molecules on stanene and stanane nanosheets—a density functional theory study. *Chem. Phys. Lett.* **695**, 162–169 (2018)
61. Rastegar, S.F., Peyghan, A.A., Hadipour, N.L.: Response of Si- and Al-doped graphenes toward HCN: a computational study. *Appl. Surf. Sci.* **265**, 412–417 (2013)
62. Prasongkit, J., Amorim, R.G., Chakraborty, S., Ahuja, R., Scheicher, R.H., Amornkitbamrung, V.: Highly sensitive and selective gas detection based on silicene. *J. Phys. Chem. C* **119**, 16934–16940 (2015)
63. Amorim, R.G., Scheicher, R.H.: Silicene as a new potential DNA sequencing device. *Nanotechnology* **26**, 154002 (2015)
64. Bhuvanewari, R., Nagarajan, V., Chandiramouli, R.: First-principles investigation on switching properties of spiropyran and merocyanine grafted graphyne nanotube device. *Chem. Phys. Lett.* **691**, 37–43 (2018)
65. Nagarajan, V., Dhivya, G., Chandiramouli, R.: First-principles investigation on transport properties of Zn₂SnO₄ molecular device and response toward NO₂ gas molecules. *J. Comput. Electron.* **17**, 1–8 (2018)
66. He, H., Scheicher, R.H., Pandey, R., Rocha, A.R., Sanvito, S., Grigoriev, A., Ahuja, R., Karna, S.P.: Functionalized nanopore-embedded electrodes for rapid DNA sequencing. *J. Phys. Chem. C* **112**, 3456–3459 (2008)
67. Büttiker, M.: Four-terminal phase-coherent conductance. *Phys. Rev. Lett.* **57**, 1761 (1986)
68. Bhuvanewari, R., Nagarajan, V., Chandiramouli, R.: Adsorption studies of trimethyl amine and n-butyl amine vapors on stanene nanotube molecular device—a first-principles study. *Chem. Phys.* **501**, 78–85 (2018)
69. Nagarajan, V., Chandiramouli, R.: Adsorption of NO₂ molecules on armchair phosphorene nanosheet for nano sensor applications—a first-principles study. *J. Mol. Graph. Model.* **75**, 365–374 (2017)

Publisher's Note Springer Nature remains neutral with regard to jurisdictional claims in published maps and institutional affiliations.